Yi, J., Lyons, P. F., Davison, P. J., Wang, P., & Taylor, P. C. (2016). Robust Scheduling Scheme for Energy Storage to Facilitate High Penetration of Renewables. *IEEE Transactions on Sustainable Energy*, *7*(2), 797-807. [7339466]. https://doi.org/10.1109/TSTE.2015.2498622

Robust Scheduling Scheme for Energy Storage to Facilitate High Penetration of Renewables

Jialiang Yi, *Student Member, IEEE*, Pádraig F. Lyons, *Member, IEEE*, Peter J. Davison, Pengfei Wang, *Student Member, IEEE*, and Philip C. Taylor, *Senior Member, IEEE*

***Abstract*—This paper presents a robust scheduling scheme for energy storage systems (ESSs) deployed in distribution networks to facilitate high penetrations of renewable energy sources (RES). This scheme schedules the charging and discharging of an ESS cognizant of state-of-charge (SoC) limits, transmission line real time thermal ratings (RTTR), and voltage constraints. Robust optimization (RO) has been adopted to deal with the uncertainty of RES output, load, and RTTR. Two methods have been introduced to estimate the tradeoff between the cost and the probability of constraint violations. The proposed scheduling scheme is tested on the IEEE 14 and 118 busbar networks with real load, generation, and RTTR profiles through Monte Carlo simulation (MCS). Test results show that the proposed scheme is able to minimize or curtail the probability of constraint violation to a desired level. In contrast, classical optimal power flow (OPF) approaches which do not consider uncertainty, when coupled with RTTR and ESS, result in a low PoS. At the same time, compared to conservative OPF approaches, the proposed scheme reduces the power and energy requirement of ESS.**

***Index Terms*—Energy storage system, renewable energy sources, robust optimization, scheduling of energy storage systems.**

NOMENCLATURE

ASHP	air source heat pump
BMS	battery management system
BoU	budget of uncertainty
DN	distribution network
ESS	energy storage system
EV	electric vehicle
LCT	low carbon technology
LF	load forecast
LMA	Levenberg-Marquardt algorithm
LO	linear optimization
LV	low voltage
MAPE	mean absolute percentage error
MCS	Monte Carlo simulation
OBoU	optimal budget of uncertainty
OPF	optimal power flow
PDF	probability density function
PFSF	power flow sensitivity factor
PoS	probability of success
RES	renewable energy sources
RMSE	root means square error
RO	robust optimization
RTTR	real time thermal rating
SoC	state-of-charge
SoH	state-of-health
STLF	short-term load forecast
UC	unit commitment
UI	uncertainty interval
ULO	uncertain linear optimisation
VSF	voltage sensitivity factor
VSTLF	very short-term load forecast

Manuscript received April 15, 2015; revised August 13, 2015; accepted October 30, 2015. Date of publication November 26, 2015; date of current version March 18, 2016. Paper no. TSTE-00302-2015.

The authors are with the School of Electrical and Electronic Engineering, Newcastle University, NE1 7RU Newcastle Upon Tyne, U.K. (e-mail: j.yi@ncl.ac.uk).

Color versions of one or more of the figures in this paper are available online at http://ieeexplore.ieee.org.

Digital Object Identifier 10.1109/TSTE.2015.2498622

I. INTRODUCTION

GOVERMENTAL policy around the world is incentivizing the decarbonization of energy infrastructure. The UK government, for example has a target of achieving an 80% reduction in CO_2 emissions with respect to the values from 1990 by 2050 [1]. Renewables based electricity generation from windfarms and photovoltaics coupled with substantial electrification of the transport and heat sectors though low carbon technologies (LCTs) such as electric vehicles (EVs) and air source heat pumps (ASHPs) will be essential to achieve this transition. The anticipated proliferation of these technologies in future energy systems will necessitate major changes to the operation and planning of future distribution networks (DNs).

Energy storage systems (ESSs) have been implemented to facilitate the uptake of RES and increase effective network capacity [2]–[5]. A rule-based control system for dispatching intermittent renewable sources is described in [2]. An approach for planning and operating grid-scale ESS to improve windfarm integration in the electricity market has been proposed previously [3]. A real-time control strategy to track the output profile of a combined RES-ESS system is described in [4]. A multi-objective optimisation approach has been used in [5] in a low voltage (LV) network for voltage control, reducing peak load and annual cost.

However, with increasing penetrations of RES and LCTs, together with the adoption of advanced network management techniques, the uncertainties associated with load forecasting (LF), generation forecasting and real time thermal rating (RTTR) will bring more opportunities and challenges to the operation and scheduling of ESSs.

Robust optimization (RO) is a modelling framework for optimization under uncertainty. The use of RO enables solving an

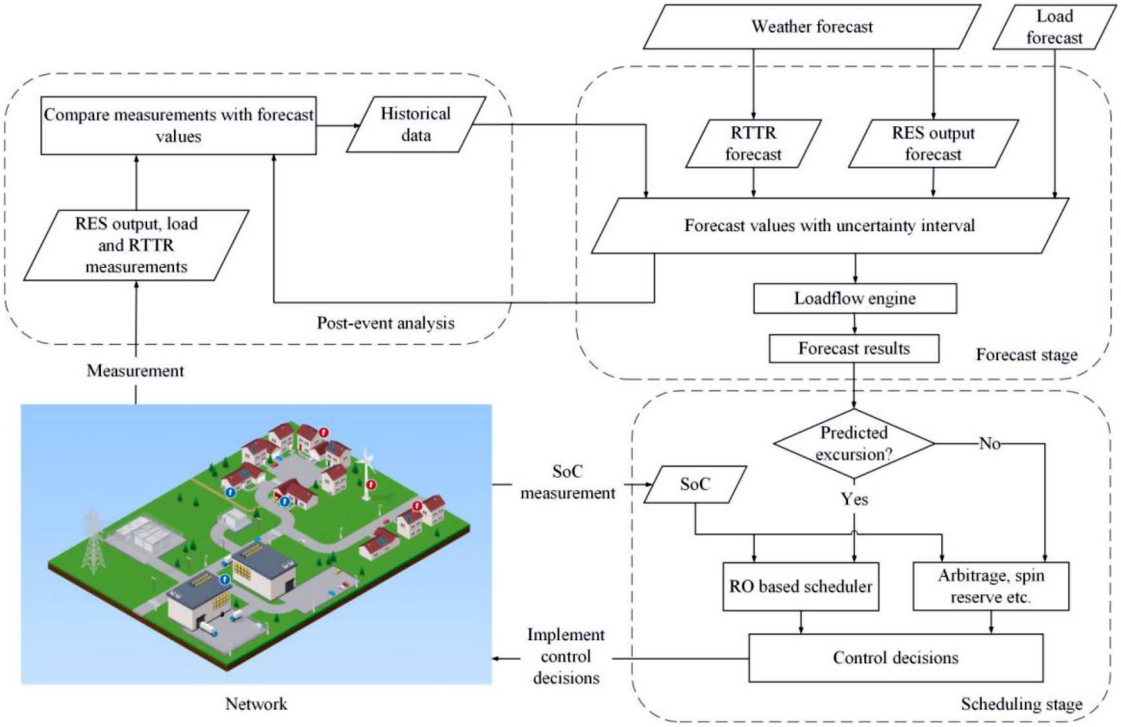

Fig. 1. Proposed Scheduling Scheme.

uncertain linear optimisation (ULO) problem deterministically. Unlike stochastic optimisation or probabilistic power flow approaches, RO does not require the probability density function (PDF) of the uncertainties.

RO has been applied previously to solve power system unit commitment (UC), network expansion planning and power dispatch problems, under the uncertainty of load, wind forecast and electricity price [6]–[8]. RO has been used to solve a look-ahead wind power problem. It has been found that the use of RO can reduce wind power curtailment and assist frequency regulation [6]. A two-stage RO based formulation for a UC problem, which incorporates a pumped-hydro storage unit to deal with wind forecast uncertainty is described in [7]. A UC problem, considering the uncertainty of node injection, has been demonstrated to be solvable with an RO approach [8]. In this work, a two-stage adaptive RO model for security constrained UC problems is formulated. A practical solution method, to solve the adaptive model, is developed and numerical experiments with real data are used to evaluate the approach.

This paper presents a scheduling scheme for ESSs in DNs. The proposed scheme is able to provide robust and adjustable solutions to avoid thermal violations, under the uncertainties of high penetrations of renewable based generation, load and RTTR. The scheduling scheme gives real power charge and discharge setpoints to the battery management system (BMS) and also informs the BMS of state-of-charge (SoC) requirements prior to the schedule period. Consequently, this scheme can assist in integrating RES whilst deferring or avoiding network reinforcement.

This paper is organized as follows. The proposed scheduling scheme is introduced in section II, followed by a review of the sources of uncertainty that can impact on the operation of a scheduling scheme. In the next section, the optimization formulation embedded in the scheduling scheme is detailed. Case study results using the IEEE 14 and IEEE 118 busbar network, under scenarios which include the uncertainty associated with the input variables to the control scheme (RTTR, load, RES generation, ESS SoC), are presented in section IV. Finally, conclusions are drawn in section V.

II. Proposed Scheduling Scheme and Sources of Uncertainty

In this section, the proposed scheduling scheme is introduced. This is followed by a review of the uncertainties that can impact on the operation of a scheduling scheme.

A. Proposed Scheduling Scheme

The proposed scheduling scheme is illustrated in Fig. 1. This scheme can be divided into three stages: Forecast stage; Scheduling stage and Post-event analysis stage.

1) Forecast Stage: Weather forecast data can be used to predict the RTTR of transformers and overhead lines and RES generation. The predicted RES generation outputs and load forecast (LF) data are used as input data to powerflow calculations.

The RO approach adopted in this paper requires an estimation of the range of uncertainty associated with these input variables. In this work, this range is called the uncertainty interval (UI). Therefore, the forecast values consist of forecast values and their UIs. In the case study presented later, the forecast values include RTTR forecast, load and RES generation forecast. However, depending on the forecast technique used

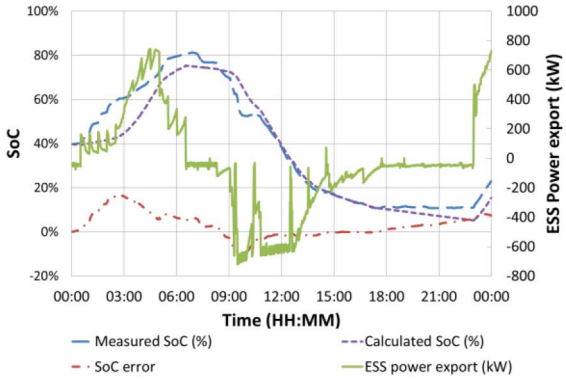

Fig. 2. ESS Measured and Calculated SoC.

and the variables of interest, UIs for each variable may not be always available. At the post-event analysis stage, historical data can be used to derive an estimation of this forecast error and can be used to derive the UI associated with this variable. This will be further explained in the description of the post-event analysis stage.

2) Scheduling Stage: At the scheduling stage, if a predicted line RTTR violation is found, based on the results from the forecast stage, RO based scheduling will be carried out. Overhead line RTTR violation prediction is based on the nominal forecast values. During the scheduling stage, SoC information from ESS will be used to inform the scheduler of the energy available. Based on this information the RO based controller can decide the import or export from ESS.

On the other hand, if there is no predicted line RTTR violation, the ESS will be made available to provide other services such as arbitrage and spinning reserve.

3) Post-Event Analysis: Finally, at the post-event stage, the real measurements of weather, generation, load and RTTR are compared to their forecast values. This comparison can be used to improve the error estimation of forecast. By improving the UIs, this feedback process can increase the robustness and reduce the conservatism of the scheme.

B. Sources of Uncertainty

Studies evaluating the prediction errors associated with forecasting wind speed, wind based generation, load and RTTR are reviewed. SoC estimation results from a real ESS trialled on a UK network are reported. Wind based distributed generation is used in this work to illustrate how RO can be used to manage the uncertainty of RES generation. It should be noted that this methodology can be applied to other type of RES.

1) Wind Speed and Wind Power Forecast: Wind speed forecast error has been shown previously to follow a Gaussian distribution [9]. However the range of the forecast error, given in root means square error (RMSE), increases with the prediction horizon. Due to the non-linear relationship between wind speed and wind power generation, the forecast error of wind power generation is asymmetrical. Previously, it has been demonstrated that the forecast error PDF is fat tailed and can be modelled by a Beta distribution [10]. In [11], two neural network based methods have been used for short term wind power generation forecast. The proposed methods construct prediction intervals with a 90% confidence level.

Wind power forecast error can be influenced by factors such as the technique used and the site. Based on the example given in [9], it is reasonable to assume that wind speed error of $+/-3\,\mathrm{m/s}$ would result in a wind power generation forecast error of less than 10% of rated power output of the wind farm.

2) Load Forecast: Short-term load forecast (STLF) and very short term load forecast (VSTLF) techniques predict the demand from the next minute to up to a number of hours. Various STLF and VSTLF techniques have been studied and compared previously [12]–[17]. Case studies indicate that depending on forecast technique, accuracy of input data, sizes of the case study networks and type of day (normal day or holidays), the uncertainty in the forecast result, given in the mean absolute percentage error (MAPE), can vary from less than 1% to more than 10%. In this work, it is assumed that load forecast uncertainty is 5%.

3) RTTR: The real time rating of overhead lines, cables and transformers are influenced by environmental conditions such as wind speed, wind direction, ambient temperature and solar irradiance. Previous work has identified that for overhead lines, wind speed has a major impact on its RTTR [18]. It has been found that 10% error in wind speed at 8 m/s can lead to an error of approximately 4% in RTTR [18].

4) SoC: A number of techniques have been developed to estimate ESS SoC including open circuit voltage or current integration method [20]. However, it is difficult to measure the SoC accurately. The SoC measurements of a 2.5MVA, 5MWh Li-Ion ESS during a field trial have been reported. This ESS is installed as part of the CLNR project [19], [20]. Fig. 2 compares the measured SoC from the battery management system and the calculated SoC based on the power import and export recorded at one minute resolution.

As can be observed, during the charge period between 00:00 to 07:00, the measured SoC is higher than the calculated SoC. During the discharge period between 09:00 to 18:00, the measured SoC is lower than that of the calculated. The error between the measured and calculated SoC reduces when the BESS is idle. The correlation coefficient between the SoC error and power export is 0.77, which indicates a relatively high correlation between the two values.

III. Formulation

The scheduling scheme and uncertainties that involved in this scheme are detailed in Section II. This section introduces the formulation of the RO based scheduling scheme. The formulation without uncertainty is introduced first. This is followed by an explanation of how the formulation is extended so that the aforementioned uncertainties can be managed.

The scheduling algorithm plans the import and export of ESS from time $t = 0$ to time $t = T$ so that line RTTR overloads and voltage violations can be avoided. This formulation uses power flow sensitivity factors (PFSF) and voltage sensitivity factors (VSF) to estimate the powerflow and voltage change due to ESS and RES. PFSFs and VSFs can be derived from the Jacobian matrix of the network under consideration [21].

A. Formulation Without Uncertainty

1) Objective Function: The objective function minimizes the cost of charging or discharging ESS during the scheduling period.

$$min \sum_{t=0}^{T} \sum_{m=1}^{N_{ESS}} C_{ESS_m} \cdot P^t_{ESS_m} \tag{1}$$

In the objective function, T is the number of timesteps, N_{ESS} is the total number of ESSs, C_{ESS_m} is the cost of charging or discharging ESS m, $P^t_{ESS_m}$ is the real power import or export of ESS m at time t. C_{ESS_m} is determined by the capital cost per kW and the state-of-health (SoH) of ESS m.

$$C_{ESS_m} = k_1 \cdot C_{ESS_m,Capital} + k_2 \cdot SoH_{ESS_m} \tag{2}$$

k_1 is a positive coefficient and k_2 is a negative coefficient. $C_{ESS_m,Capital}$ is the capital cost of ESS m and SoH_{EES_m} is the SoH of ESS m. By varying the weight factors k_1 and k_2, this cost function enables a trade-off between the capital cost and the SoH of an ESS. SoH can be quantified by the number of cycles left before the remaining capacity of the system deteriorates to 80%.It should be noted that C_{ESS_m} is not the actual cost of using an ESS.

2) Constraints: Constraints in this paper include powerflow constraints, voltage constraints and ESS SoC constraints.

- Powerflow constraint

$$-S^t_{ij,RTTR} \le S^t_{ij,Estimate} \le S^t_{ij,RTTR} \tag{3}$$

In which $S^t_{ij,RTTR}$ is the RTTR of branch from bus i to bus j (branch ij) at time t, $S^t_{ij,Estimate}$ is the estimated powerflow on branch ij and is given by

$$\begin{aligned} S^t_{ij,Estimate} = {} & S^t_{ij,Forecast} \\ & + \sum_{m=1}^{N_{ESS}} PFSF^t_{ij,ESS_m} \cdot P^t_{ESS_m} \\ & + \sum_{n=1}^{N_{RES}} PFSF^t_{ij,RES_n} \cdot \Delta P^t_{RES_n} \\ & + \sum_{p=1}^{N_{Bus}} PFSF^t_{ij,Bus_p} \cdot \Delta P^t_{Bus_p} \end{aligned} \tag{4}$$

$S^t_{ij,Forecast}$ is the forecasted powerflow of branch ij at time t, based on powerflow calculations at the forecast stage, $PFSF^t_{ij,ESS_m}$, $PFSF^t_{ij,RES_n}$ and $PFSF^t_{ij,Bus_p}$ is the PFSF of ESS m, RES n and busbar p to branch ij at time t, which represents the apparent power change (in MVA) through branch ij due to per MW real power change from ESS m, RES n and busbar p. $\Delta P^t_{RES_n}$ and $\Delta P^t_{Bus_p}$ is the error of RES power output and busbar load. In this formulation, only the power output and busbar load forecast error is used. The reason is explained below. If the actual power output of RES and the busbar load at time t is given by

$$P^t_{RES_n} = P^t_{RES_n,Forecast} + \Delta P^t_{RES_n} \tag{5}$$

$$P^t_{Bus_p} = P^t_{Bus_p,Forecast} + \Delta P^t_{Bus_p} \tag{6}$$

At the forecast stage, $P^t_{RES_n,Forecast}$ and $P^t_{Bus_p,Forecast}$ are used to calculate $S^t_{ij,Forecast}$ and as a result, to estimate the powerflow on branch ij at time t, only the forecast error $\Delta P^t_{RES_n}$ and $\Delta P^t_{Bus_p}$ is needed.

The use of sensitivity factor is a linearization of the non-linear powerflow equations. It is found in [22] that, PFSFs are only insensitive to the operating point in networks with sufficient voltage support. With the increasing penetrations of RES and future load, voltage profiles of distribution networks will be more volatile. In this work, the PFSFs are calculated based on loadflow equations with updated load and generation values for each timestep to enhance the accuracy.

Constraint (3) is only applied to branches with high PFSF from ESS or renewables to reduce the size of the problem.

- Voltage constraint

$$\begin{aligned} V_{Min,i} \le {} & V^t_{i,Forecast} + \sum_{m=1}^{N_{ESS}} VSF^t_{i,ESS_m} \cdot P^t_{ESS_m} \\ & + \sum_{n=1}^{N_{RES}} VSF^t_{i,RES_n} \cdot \Delta P^t_{RES_n} \\ & + \sum_{p=1}^{N_{Bus}} VSF^t_{i,Bus_p} \cdot \Delta P^t_{Bus_p} \le V_{Max,i} \end{aligned} \tag{7}$$

$V_{Min,i}$ and $V_{Max,i}$ are the lower and upper voltage limits of busbar i. $V^t_{i,Forecast}$ is the forecasted voltage of busbar i at time t based on powerflow calculations. VSF^t_{i,ESS_m}, VSF^t_{i,RES_n} and VSF^t_{i,Bus_p} is the voltage sensitivity factor which denotes the voltage change of busbar i due to the power change of ESS, RES and load at time t.

This constraint guarantees that all busbar voltages are within limits. Similar to powerflow constraints, only critical busbars with high VSFs from ESS will be added to this constraint.

- ESS SoC constraint

The SoC of ESS is calculated by (8).

$$\begin{aligned} SoC^{t+1}_{ESS_m} = {} & SoC^t_{ESS_m} + d^t \cdot \frac{\Delta t \cdot \frac{P^t_{ESS_m}}{\eta_{ESS_m,discharge}}}{E_{ESS_m}} \\ & + \left(1 - d^t\right) \cdot \frac{\Delta t \cdot P^t_{ESS_m} \cdot \eta_{ESS_m,charge}}{E_{ESS_m}} \end{aligned} \tag{8}$$

$SoC^t_{ESS_m}$ and $SoC^{t+1}_{ESS_m}$ is the SoC of ESS at time t and $t+1$. Δt is the duration of each timestep. $\eta_{ESS_m,discharge}$ and $\eta_{ESS_m,charge}$ is the efficiency of ESS m during discharge and charge. d is a binary variable, $d = 1$ if discharge and $d = 0$ if charge, E_{ESS_m} is the energy capacity of the ESS m.

The next constraint prevents the ESS from over charge or over discharge

$$SoC^t_{ESS_m,Min} \le SoC^t_{ESS_m} \le SoC^t_{ESS_m,Max} \tag{9}$$

$SoC^t_{ESS_m,Min}$ and $SoC^t_{ESS_m,Max}$ is the minimum and maximum SoC limit for ESS m at time t.

This ESS scheduling problem can be generalized as a linear optimization (LO) problem

$$minf\left(\boldsymbol{P}_{ESS}^{t}\right) \tag{10}$$

Subject to

$$\boldsymbol{l} \leq \boldsymbol{h}\left(\boldsymbol{P}_{ESS}^{t}, \Delta\boldsymbol{P}_{RES}^{t}, \Delta\boldsymbol{P}_{Bus}^{t}, \boldsymbol{S}_{Branch,Forecast}^{t}, \boldsymbol{V}_{Bus}^{t}, \boldsymbol{SoC}_{ESS}^{t=0}\right) \leq \boldsymbol{u} \tag{11}$$

$$\boldsymbol{g}\left(\boldsymbol{P}_{ESS}^{t}, \boldsymbol{SoC}_{ESS}^{t=0}\right) = \boldsymbol{0} \tag{12}$$

Where:

- $\boldsymbol{h}$ is the function for inequality constraints
- $\boldsymbol{g}$ is the function for equality constraints
- $\boldsymbol{l}$ and $\boldsymbol{u}$ is the lower and upper limit

By finding a feasible solution $\boldsymbol{P}_{ESS}^{t}$, this formulation minimizes the cost of charging and discharge the ESS whilst simultaneously eliminating the risk of line RTTR overload, voltage limit violations and over-charge or over-discharge of ESS. The equality constraints calculate the SoC of the ESS from time $t = 0$ to time $t = T$. The inequality constraints include powerflow constraints, voltage constraints and SoC constraints.

B. Formulation With Uncertainty and Budget of Uncertainty

Considering the aforementioned uncertain inputs, the objective function remains the same. The constraints given in (11) and (12) become

$$\boldsymbol{l} \leq \boldsymbol{h}\left(\boldsymbol{P}_{ESS}^{t}, \Delta\tilde{\boldsymbol{P}}_{RES}^{t}, \Delta\tilde{\boldsymbol{P}}_{Bus}^{t}, \tilde{\boldsymbol{S}}_{Branch,Forecast}^{t}, \boldsymbol{V}_{Bus}^{t}, \widetilde{\boldsymbol{SoC}}_{ESS}^{t=0}\right) \leq \boldsymbol{u} \tag{13}$$

$$\boldsymbol{g}\left(\boldsymbol{P}_{ESS}^{t}, \widetilde{\boldsymbol{SoC}}_{ESS}^{t=0}\right) = \boldsymbol{0} \tag{14}$$

(13) and (14) form an uncertain linear optimization problem. In this work, it is assumed that all uncertain values are independent and each uncertainty variable a is bounded by an interval given as

$$\tilde{a} \in [a - \hat{a}, a + \hat{a}] \tag{15}$$

Where $\tilde{a}$ is the real value of a and $\hat{a}$ is the maximum error. Thus, the general form of (13) and (14) can be given as

$$\sum \tilde{a}_{ij} \cdot x \leq b \tag{16}$$

This uncertain linear optimization problem is solved by the methodology proposed in [23]. Each line of the constraints, where uncertainty exists, can be reformed so that it can be solved as a normal linear optimization problem. The set of all $\tilde{a}_{ij}$ is denoted as J_i. Next, it is assumed, up to $\lfloor\Gamma_i\rfloor$ number of a_{ij} are uncertain and $-\hat{a} \leq \tilde{a}_{ij} - a_{ij} \leq \hat{a}$, $\lfloor\Gamma_i\rfloor$ is the floor of Γ_i which means $\lfloor\Gamma_i\rfloor$ is the largest integer not greater than Γ_i. This set of uncertainties is denoted by S and $|S| = \lfloor\Gamma_i\rfloor, S_i \subseteq J_i$. One coefficient changes by $(\Gamma_i - \lfloor\Gamma_i\rfloor)\,\hat{a}_{it}$, this uncertainty is recorded as t_i and $t_i \in J_i \backslash S_i$

$$\sum_j a_{ij}x_j + \max_{\{S_i \cup \{t_i\} | S_i \subseteq J_i, |S_i| = \lfloor\Gamma_i\rfloor, t_i \in J_i \backslash S_i\}} \left\{\sum_{j \in S_i} \hat{a}_{ij}y_j + (\Gamma_i - \lfloor\Gamma_i\rfloor)\,\hat{a}_{it_i}y_t\right\} \leq b_i$$
$$-y_{ij} \leq x_j \leq y_{ij} \quad \forall i, j \in J_i$$
$$\boldsymbol{y} \geq \boldsymbol{0} \tag{17}$$

An additional parameter Γ_i^t, has been introduced into (17). This parameter Γ_i^t is called budget of uncertainty (BoU) and is used to adjust the conservatism of the solution. BoU can be understood as the number of uncertainties the constraints can be protected against. Denoting the total number of uncertain values in (17) as N_u, BoU has a minimum value of 0 and a maximum of N_u.

$$0 \leq \Gamma_i^t \leq N_u \tag{18}$$

When BoU is 0, (17) becomes a normal liner optimization problem. When BoU equals N_u, (17) becomes

$$\sum_j a_{ij}x_j + \sum_{j=0}^{N_u} \hat{a}_{ij}y_j \leq b_i - y_{ij} \leq x_j \leq y_{ij}$$
$$\forall i, j \in J_i \; \boldsymbol{y} \geq \boldsymbol{0} \tag{19}$$

(19) is the worst case for (16) and as a result, a feasible solution of (19) is immune to all the defined uncertainties. When BoU Γ_i^t is an integer, the constraint can be protected when up to Γ_i^t uncertain values and $a - \hat{a} \leq \tilde{a} \leq a + \hat{a}$. When BoU is not an integer, the constraint is safe when up to $\lfloor\Gamma_i^t\rfloor$ values are uncertain and $a - \hat{a} \leq \tilde{a} \leq a + \hat{a}$ and one value follows $a - (\Gamma_i^t - \lfloor\Gamma_i^t\rfloor)\,\hat{a} \leq \tilde{a} \leq a + (\Gamma_i^t - \lfloor\Gamma_i^t\rfloor)\,\hat{a}$. Even if more than Γ_i^t values are uncertain, the solution based on this BoU still provides a high probability that constraint violations can be avoided through the use of ESS. For instance, the right-hand side of (3) at time t is given as

$$S_{ij,Forecast}^{t} + \sum_{n=1}^{N_{ESS}} PFSF_{ij,ESS_m}^{t} \cdot P_{ESS_m}^{t} + \sum_{n=1}^{N_{RES}} PFSF_{ij,RES_n}^{t} \cdot \Delta\tilde{P}_{RES_n}^{t} + \sum_{p=1}^{N_{Bus}} PFSF_{ij,Bus_p}^{t} \cdot \Delta\tilde{P}_{Bus_p}^{t} \leq \tilde{S}_{ij,RTTR}^{t} \tag{20}$$

Considering the uncertainty of RES, load forecast and RTTR, (20) becomes

$$S_{ij,Forecast}^{t} + \sum_{n=1}^{N_{ESS}} PFSF_{ij,ESS_m}^{t} \cdot P_{ESS_m}^{t} + \sum_{n=1}^{N_{RES}} PFSF_{ij,RES_n}^{t} \cdot \Delta\tilde{P}_{RES_n}^{t} + \sum_{p=1}^{N_{Bus}} PFSF_{ij,Bus_p}^{t} \cdot \Delta\tilde{P}_{Bus_p}^{t} \leq \tilde{S}_{ij,RTTR}^{t} \tag{21}$$

Where, $\tilde{S}^t_{ij,RTTR}$, $\Delta\tilde{P}^t_{RES_n}$ and $\Delta\tilde{P}^t_{Bus_p}$ is the uncertainty value of predicted RTTR of branch ij, predicted power output of RES n and load forecast of busbar p at time t, respectively The total number of uncertainties is $N_u = N_{RES} + N_{Bus} + 1$. For this constraint, BoU means how many of these forecast values will be greatly deviate from their nominal values, in other words, their real values $\tilde{a}_{ij}$ will be close or equal to their lower or upper bounds.

For simplicity, the rest of the paper uses normalized value Γ/N_u to represent the BoU. Increasing the BoU will reduce the probability of constraints violation or increase the probability of success (PoS) of the solution. PoS is defined as

$$PoS = \left(1 - \frac{N_{Vio}}{N_{Total}}\right) \times 100\% \tag{22}$$

N_{Total} is the total number of Monte Carlo samples and N_{Vio} is the number of violations recorded.

The selection of BoU is critical to the performance of the algorithm. A high BoU ensures high PoS however can be over-conservative. A low BoU reduces the cost but also lowers the PoS. In the following section, two approaches are introduced to estimate the PoS of a given BoU.

C. PoS Estimation Technique

The first approach is based on [23]. Based on this work the relationship between PoS and BoU can be represented by

$$PoS \geq 1 - \exp\left(-\frac{\Gamma_i^2}{2 \cdot N_u}\right) \tag{23}$$

This function describes how PoS changes with BoU. However, this estimate is based on the assumption that the errors are symmetrically distributed regardless of the type of distribution. The limitation of this estimation is that the estimated PoS is conservative and less accurate when the number of uncertainties N_u is small.

The second approach introduces extra parameters into (23) and it becomes

$$PoS = a - b \cdot \exp\left(-c \cdot \Gamma_i^2\right) \tag{24}$$

It can be shown that (24) is a modification of (23). By calculating the values of a, b and c, the relationship between Γ and PoS can be adjusted. The values of a, b and c can be calculated by using curve fitting techniques. To calculate the values of the parameters, only three inputs and outputs, Γ and corresponding PoS, are required. The PoS of a given BoU can be achieved by running Monte Carlo simulation (MCS). This method is further discussed in the case study section. The process for this approach is illustrated below in Fig. 3.

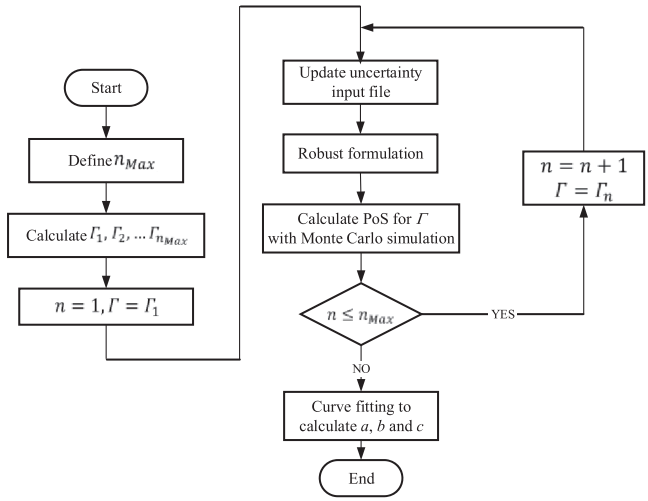

Fig. 3. Calculation of BoU Based on Curve Fitting.

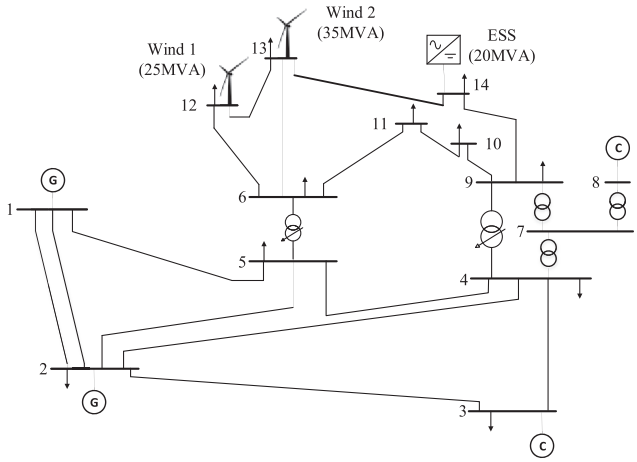

Fig. 4. IEEE 14 Busbar network.

IV. Case Study

A. Case Study on IEEE 14 Busbar Network

Tests are carried out with the IEEE 14 busbar network. A schematic of the modified network is given in Fig. 4. Windfarms, Wind 1 and Wind 2, are connected to busbars 12 and 13 with capacities of 25MVA and 35MVA, respectively. A 20 MVA, 40MWh ESS is placed at busbar 14. Wind generation at busbar 12 and 13 causes a continuous overload on the branch from busbar 13 to busbar 14. It is assumed that this branch is equipped with RTTR. In this case study, half-hourly real windfarm generation export, RTTR and load profile data from the north east of England have been used [24].

Only real power export is considered here. This method is able to solve scheduling problems with reactive power by replacing the real power injections in the constraints by apparent power injection and apparent power PFSF (MVA powerflow change per MVA injection change).

The sources of uncertainty considered in this case study include load, RES output and RTTR. The uncertainty intervals are given in Table I. The UIs in this table are defined based on literature provided in section II.B.

Three test cases have been used to test the performance of the proposed scheduling scheme with different types of uncertainty distribution. In case 1 and 2, it is assumed that all errors are symmetrically distributed and follow normal and uniform distribution, respectively. In case 3, both left and right skewed Beta

TABLE I
SOURCES OF UNCERTAINTY AND UNCERTAINTY INTERVALS

	Load	RTTR	Wind 1	Wind 2
Uncertainty interval	5%	5%	10%	10%

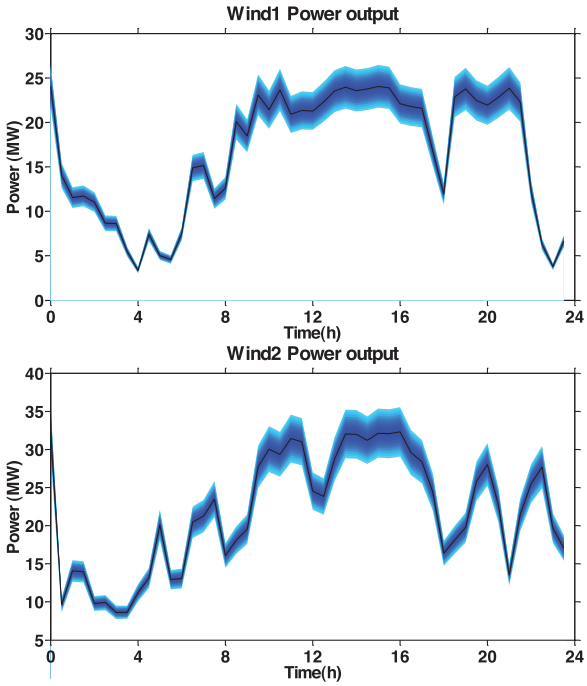

Fig. 5. Windfarm Output.

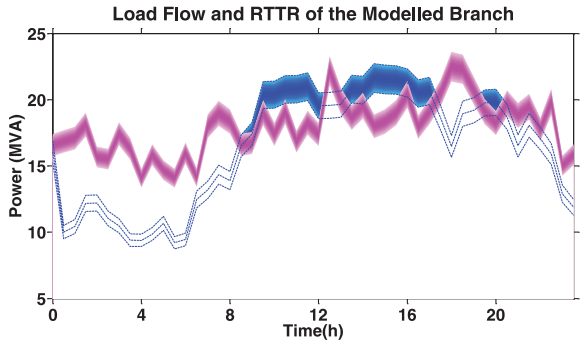

Fig. 6. Apparent Power and RTTR of the Modelled Branch.

TABLE II
SOURCES OF UNCERTAINTY AND UNCERTAINTY INTERVALS

	Load	RTTR	Wind 1	Wind 2
Uncertainty interval	5%	5%	10%	10%
Case 1 (SD/Mean)	1%	1%	2%	2%
Case 2 (Maximum variation)	5%	5%	10%	10%
Case 3 (α, β)	2, 1.5	2, 4	2, 1.5	2, 1.5

TABLE III
INPUT VALUES FOR THE CURVE FITTING ALGORITHM

Input value	Case 1		Case 2		Case 3	
	BoU	PoS	BoU	PoS	BoU	PoS
1	0%	93.44%	0%	12.46%	0%	1.06%
2	10%	99.96%	15%	79.16%	15%	69.30%
3	15%	100.0%	30%	99.82%	30%	100.0%
4	20%	100.0%	45%	100.0%	45%	100.0%

distributions have been used. The skewness of each error distribution is chosen so that the severity of violation is worse. For example, it is assumed that RTTR tends to be overestimated and wind speeds are likely to be underestimated. Beta distributions are used as the asymmetrical test case due to its simplicity.

The specifications of the distributions in the test cases are given below. For case 1, the ratio of standard deviation (SD) to mean is given. In this case, the UI is five times the SD. For case 2, the maximum variation of uniform distribution is given as a percentage. For case 3, the parameters α and β for the Beta distributions are given. The minimum and maximum value of Beta distribution function is 0 and 1. Then the data is scaled to match the defined UIs.

The windfarm export profiles and uncertainty intervals are depicted in Fig. 5. The black traces are the nominal wind generation exports and the blue shaded area surrounding the trace represents the forecast error bounds.

Powerflow through the branch and the RTTR of the branch are given in Fig. 6. The red curve with shaded area is the RTTR of the branch. The blue curve with the shaded area is the predicted powerflow through the branch with the uncertainty of load and RES. Three distinct sustained branch overloads can be observed. The scheduling scheme has been applied for the period between 04:00 to 13:00 at a half-hour interval. The total number of timesteps is 18.

B. Estimation of OBoU

To reduce the cost of using ESS and the required energy throughput, it is crucial to use a BoU that is not excessively conservative. In this work, the minimum BoU which guarantees the required PoS is defined as the optimal BoU (OBoU). In the UK, for single and multi-circuit supply systems, the aggregate percentage of time when the design temperature of the conductor can be exceeded is 0% and 3% [25], [26]. This standard is adopted by UK DNOs for operating the system with static ratings. To be consistent with this approach, in this paper, PoS targets of 100% and 97% have been used.

Due to the relatively small number of forecast values used in this case study, only the curve fitting based technique is used to calculate OBoU. The value of a, b and c are calculated with curve fitting toolbox in MATLAB. The curve fitting technique is Levenberg-Marquardt algorithm (LMA), which is normally used to solve non-linear least square problems.

For each case, four groups (n_{Max}) of BoU and its PoS have been used to calculate the parameters a, b and c in (24). The inputs used are given below in Table III.

The function describing the relationship between PoS and BoU, as given in (24), can be established with the input values in Table III. The input PoS is achieved by MCS. The parameters used for MCS are consistent with the specification given in Table II. The uncertain values used in MCS have not been truncated even though RO uses the intervals as input. MCS is carried out for all three cases for all 18 timesteps and each timestep is tested with 5,000 samples. Analysis shows

TABLE IV
ESTIMATED OBOU FOR 97% AND 100% POS

PoS	Estimated OBoU		
	Case 1	Case 2	Case 3
97%	4.0%	23.0%	26.0%
100%	9.8%	31.0%	32.0%

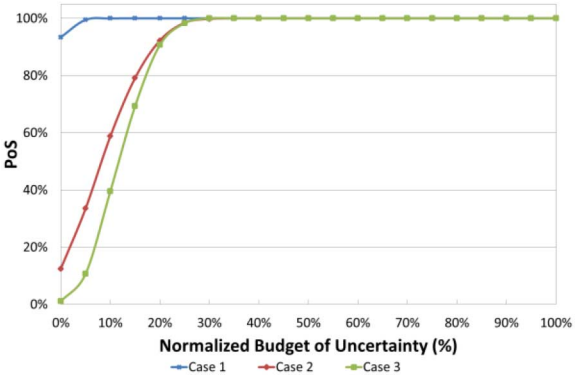

Fig. 7. PoS in the test cases.

that result converges at around 2,000 samples. Techniques for reducing the sample size of MCS are available however this is beyond the scope of this paper. The sample size is selected to guarantee the convergence of the results. The OBoU for 97% and 100% PoS can be calculated based on these functions. The estimated OBoUs are given below in Table IV.

C. Simulation Results

1) Verification of OBoU: Next, additional PoSs for more BoUs in all three cases are tested with MCS. Initially the PoS of each case was tested with MCS for normalized BoU from 0% to 100% at a 5% interval. Next, more tests were conducted for BoU with PoS of more than 90% at 1% BoU interval. Test results are illustrated in Fig. 7. As can be observed, in all cases, PoS increase with BoU. At the same BoU, the PoSs for the normal distribution case is higher in comparison with the uniform and Beta distribution cases.

Curve fitting results for Case 1 is given below in Fig. 8 as an example. The red curve depicts the results from MCS. The green dots indicate the input for curve fitting algorithm. The blue curve is the curve fitting result. The original curve and the fitting results have a high correlation coefficient of 0.9624.

The OBoU based on MCS study are summarized below in Table V. Due to the large sample size of MCS, the OBoU obtained can be seen as the real OBoU. Comparing the estimated OBoU listed in Table IV to the real OBoU in Table V, it can be seen that the curve fitting based approach can provide a good estimation of OBoU. Moreover, this method can reduce the computational cost of running MCS. In case 1 and 2, 15 and 19 steps of MCS are required. By adopting this method, the computational cost is reduced to between 20% and 30%.

2) Comparison to Optimal Power Flow: The proposed method is compared to two forms of optimal power flow (OPF) scheduling schemes, nominal OPF (NOPF) and conservative OPF (COPF). NOPF uses the nominal as input and therefore

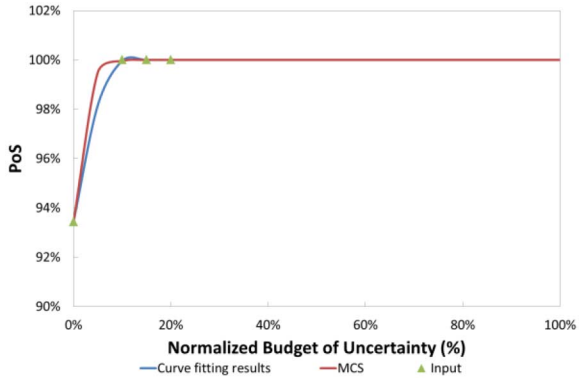

Fig. 8. Curve fitting results of test case 1.

TABLE V
OPTIMAL BOU FOR 97% AND 100% POS

PoS	OBoU		
	Case 1	Case 2	Case 3
PDF type	Normal	Uniform	Beta
97%	2%	24%	21%
100%	15%	32%	29%

TABLE VI
POS TEST RESULTS

Test	PoS		
	Case 1	Case 2	Case 3
NOPF	60.72%	41.52%	11.40%
97% Estimated OBoU	98.90%	95.97%	98.0%
100% Estimated OBoU	99.96%	99.90%	100.0%
COPF	100%	100%	100%
100% BoU	100%	100%	100%

does not consider any uncertainty. On the other hand, COPF considers the worst case scenario. In this case, COPF uses the maximum possible wind speed and minimum RTTR. The PoSs of the calculated OBoU and OPF approaches are tested with MCS. Test results are summarized in Table VI. As can be observed, without considering the uncertainty, a normal OPF approach (NOPF) results in low PoS. Meanwhile, the estimated OBoU is able to provide reliable solutions. The error of curve fitting results can be further reduced by the use of an improved selection and a larger number of input values. It can be observed that the proposed method is able to calculate the OBoU for a desired PoS. Therefore the level of conservatism can be adjusted.

Charge and discharge profiles in Case 1 for COPF, NOPF, and the RO scheme with 100% and 97% PoS are compared in Fig. 9. As shown in this figure, compared to COPF, the proposed scheme can reduce the maximum discharge power from 11 MW to 9 MW and also ensuring that the constraints are fully protected against uncertainty.

The SoC change during this period is compared in Fig. 10. During the discharge period between 09:00 to 13:00, compared to COPF, the SoC requirement can be reduced by 9.9MWh and 5.6MWh at 97% and 100% PoS.

The maximum discharge power and the SoC change for 97% and 100% PoS in all test cases are listed in Table VII. As can be observed, instead of scheduling the system for 100% PoS,

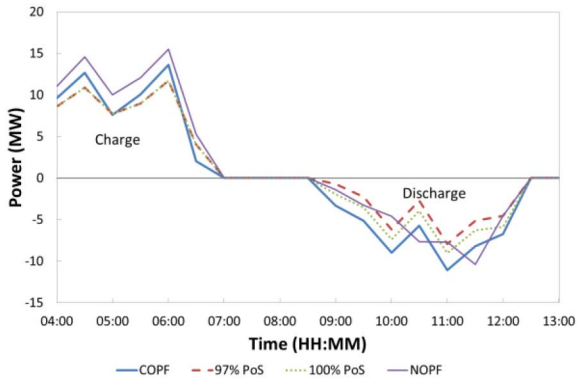

Fig. 9. ESS Charge and Discharge Profiles in Case 1.

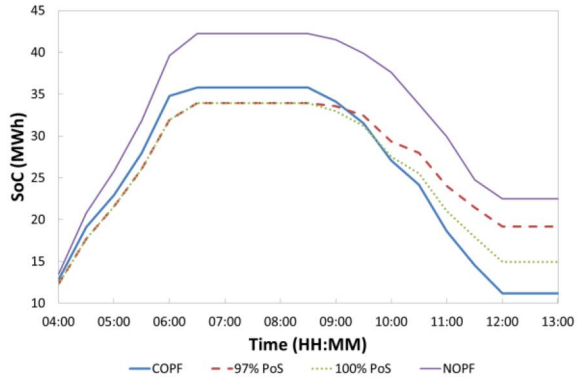

Fig. 10. SoC Comparison in case 1.

TABLE VII
PoS of Estimated OBoU

	Maximum Discharge (MW)			ΔSoC (MWh)		
	Case 1	Case 2	Case 3	Case 1	Case 2	Case 3
NOPF	10.40	10.40	10.40	19.76	19.76	19.76
97%	7.90	9.80	9.54	14.75	22.37	21.24
100%	9.00	10.41	10.18	19.00	25.26	24.19
COPF	11.10	11.10	11.10	24.6	24.6	24.6
100% BoU	13.66	13.66	13.66	32.96	32.96	32.96

a reduced requirement of 97% can reduce the required rated power and energy capacity of ESS. Meanwhile, the modest use decelerates the degradation of existing ESS.

During the first predicted line RTTR overload from 08:30 to 12:00, wind energy from RESs are 190.9MWh. Line RTTR overload can result in windfarms tripping or curtailment. Based on nominal forecast values, 26.4MWh of wind energy will be curtailed to avoid line rating violation. Under worst case scenario where branch 13 to 14 has its minimum RTTR, 83.8MWh of wind energy will be curtailed.

D. Case Study on IEEE 118 Busbar Network

The proposed scheduling scheme is applied to IEEE 118 busbar network. 6 ESSs and 10 RESs have been connected. It is assumed that all busbars have uncertain load. The uncertainty intervals are consistent with previous study on the 14 busbar network. In this case study, both OBoU estimation approaches introduced in section III.C have been used. Based on the first approach, the estimated OBoU for 100% PoS is 45.6%. The curve fitting based approach, approach 2 is used to calculate OBoU for all three cases as well. Based on the estimated BoU, charging and discharging profiles for all six ESSs can be calculated. Next, the PoS for the solutions based on different methods are evaluated through MCS. The test results for 100% PoS are summarized below in Table VIII.

TABLE VIII
PoS Results for 100% PoS

	PoS		
	Case 1	Case 2	Case 3
NOPF	48.96%	48.76%	13.90%
Approach 1 – 100%	100.0%	100.0%	99.98%
Approach 2 – 100%	100.0%	100.0%	100.0%
COPF	100.0%	100.0%	100.0%

TABLE IX
Cost Results

	PoS		
	Case 1	Case 2	Case 3
NOPF	28.8%	28.8%	28.8%
Approach 1 – 100%	96.5%	96.5%	96.5%
Approach 2 – 100%	81.5%	88.3%	89.1%
COPF	1	1	1

As can be observed, both OBoU estimation approaches can guarantee high PoS. Meanwhile, the costs for all the approaches are compared below. COPF has the highest cost. The costs for NOPF and RO based methods are given as the percentage of COPF cost.

As can be observed in Table IX, the RO based approach can provide solutions with high PoS and also reduce the cost. The reason RO can provide solutions with high PoS and reduced cost is that, COPF considers the worst case scenario, which means all uncertain values take values at their lower or upper bounds. However, it is unlikely that all uncertain values take values near their lower or upper bounds. On the other hand, the proposed scheme is able to realize the trade-off between the cost and the probability of constraint violations. Therefore the requirements for ESS power and energy rating can be reduced.

V. Discussion

The proposed scheduling scheme presents several advantages compared to stochastic optimization and chance constraint techniques. In scenarios where, for uncertain values, only their UIs exist or their PDFs are only partially available or even inaccurate, techniques such as stochastic optimization or chance-constraint programming are unable to solve the problem. On the other hand, it has been shown that the proposed RO based scheduling scheme is still able to provide robust solutions to avoid branch line RTTR violation, cognizant of ESS SoC limits and network voltage constraints. In such scenarios, approach 1 based on (23) is able to provide robust solutions based on simple calculations in a very short time even for a large network. In scenarios where accurate PDFs are available for all the uncertain values, the advantages of RO based scheduling scheme still exist. Under such circumstances, both the estimation and the curve fitting based approaches can

be used to calculate OBoU. The estimation approach can be applied to calculate a slightly conservative but robust solution in a very short time. Curve fitting based approach constructs the function between BoU and PoS through MCS. MCS runs a large number of load flow calculations to compute the PoS at different BoU. The MCS process is time consuming however it avoids any linearization of the network model. As a result, the curve fitting method is able to provide accurate solutions and ensure desired levels of PoS. The capability of adjusting the PoS is beneficial to the future deployment of ESS. As shown in the simulation results, by accepting a PoS requirement of 97%, the proposed method can further reduce the power and energy requirements of ESS.

The selection of UI is important to the performance of RO. Forecast techniques for UI prediction have been proposed [11], [27], [28]. Conservative UIs can compromise the benefits of the proposed approach. On the other hand, if the uncertainty is underestimated, the PoS of RO solutions will be reduced.

VI. Conclusion

This paper describes a new application of RO for solving an ESS scheduling problem considering new sources of uncertainty, namely the uncertainty of RTTR and ESS SoC. The scheduling of ESS, compared to aforementioned RO applications, involves bidirectional powerflows and is constrained by the available energy resource from ESS. The formulation proposed in this paper considers the SoC constraint so that ESSs, which are currently expensive and fragile, can be protected from over-charging and over-discharging. Furthermore, the proposed cost function takes into account the capital cost and the SoH of different ESSs. The uncertainty of RTTR is influenced by a number of factors including model limitations and measurement accuracy of environmental factors such as wind speed and direction. Therefore, developing appropriate PDFs for RTTR in large networks is almost an impossible task. This poses difficulties for techniques that demand PDFs.

The proposed RO scheduling scheme is compared to OPF techniques. Reliability test results through MCS with 5,000 samples for all scheduled timesteps on IEEE 14 and 118 busbar networks with real wind, load and RTTR data are presented. Test results show that classical OPF approaches which do not consider uncertainty, when coupled with RTTR and ESS, result in a low PoS In comparison with COPF, which also provides high PoS, the proposed RO scheduling scheme is able to reduce the power and energy requirement to solve a line RTTR violation under uncertainty. The reduced ESS requirements would reduce the power rating and energy capacities required for the ESS and slow the cyclic degradation of the system.

In addition, two methods have been introduced to estimate the trade-off between the cost and the probability of constraint violations. The first approach results in a slightly conservative solution for small networks. When applied to a large network, the approach can reduce the requirements for ESS power rating and energy capacity. The second approach, which uses a moderate number of MCSs coupled with LMA curve fitting technique, has been proposed to estimate the optimal BoU, to ensure a desired level of PoS. Simulation results show that, the proposed methodology is able to provide an ESS charge and discharge profile that ensures a desired level of probability of success. It has also been found that, reducing the PoS requirement from 100% to 97%, the proposed method can further reduce the power and energy requirements of ESS. The case study results show that, reducing the PoS requirement by 3% reduces the capacity requirement of ESS by up to 4.25 MWh. The scheme proposed in this paper provides a practical solution to ESS scheduling problems under uncertainty to facilitate high penetrations of RES.

References

[1] U.K. Parliament, *Climate Change Act 2008*. London, U.K.: HMSO, 2008.

[2] S. Teleke, M. E. Baran, S. Bhattacharya, and A. Q. Huang, "Rule-based control of battery energy storage for dispatching intermittent renewable sources," *IEEE Trans. Sustain. Energy*, vol. 1, no. 3, pp. 117–124, Oct. 2010.

[3] M. Dicorato, G. Forte, M. Pisani, and M. Trovato, "Planning and operating combined wind-storage system in electricity market," *IEEE Trans. Sustain. Energy*, vol. 3, no. 2, pp. 209–217, Apr. 2012.

[4] A. Damiano, G. Gatto, I. Marongiu, M. Porru, and A. Serpi, "Real-time control strategy of energy storage systems for renewable energy sources exploitation," *IEEE Trans. Sustain. Energy*, vol. 5, no. 2, pp. 567–576, Apr. 2014.

[5] J. Tant, F. Geth, D. Six, P. Tant, and J. Driesen, "Multiobjective battery storage to improve PV integration in residential distribution grids," *IEEE Trans. Sustain. Energy*, vol. 4, no. 1, pp. 182–191, Jan. 2013.

[6] W. Wenchuan, C. Jianhua, Z. Boming, and S. Hongbin, "A robust wind power optimization method for look-ahead power dispatch," *IEEE Trans. Sustain. Energy*, vol. 5, no. 2, pp. 507–515, Apr. 2014.

[7] J. Ruiwei, W. Jianhui, and G. Yongpei, "Robust unit commitment with wind power and pumped storage hydro," *IEEE Trans. Power Syst.*, vol. 27, no. 2, pp. 800–810, May 2012.

[8] D. Bertsimas, E. Litvinov, X. A. Sun, Z. Jinye, and Z. Tongxin, "Adaptive robust optimization for the security constrained unit commitment problem," *IEEE Trans. Power Syst.*, vol. 28, no. 1, pp. 52–63, Feb. 2013.

[9] M. Lange, "On the uncertainty of wind power predictions—analysis of the forecast accuracy and statistical distribution of errors," *J. Solar Energy Eng.*, vol. 127, pp. 177–184, 2005.

[10] H. Bludszuweit, J. A. Dominguez-Navarro, and A. Llombart, "Statistical analysis of wind power forecast error," *IEEE Trans. Power Syst.*, vol. 23, no. 3, pp. 983–991, Aug. 2008.

[11] A. Khosravi, S. Nahavandi, and D. Creighton, "Prediction intervals for short-term wind farm power generation forecasts," *IEEE Trans. Sustain. Energy*, vol. 4, no. 3, pp. 602–610, Jul. 2013.

[12] M. Alamaniotis, A. Ikonomopoulos, and L. H. Tsoukalas, "Evolutionary multiobjective optimization of kernel-based very-short-term load forecasting," *IEEE Trans. Power Syst.*, vol. 27, no. 3, pp. 1477–1484, Aug. 2012.

[13] Z. Rui, D. Zhao Yang, X. Yan, M. Ke, and W. Kit Po, "Short-term load forecasting of Australian national electricity market by an ensemble model of extreme learning machine," *IET Gener. Transm. Distrib.*, vol. 7, pp. 391–397, 2013.

[14] K. Nose-Filho, A. D. P. Lotufo, and C. R. Minussi, "Short-term multinodal load forecasting using a modified general regression neural network," *IEEE Trans. Power Del.*, vol. 26, no. 4, pp. 2862–2869, Oct. 2011.

[15] F. Shu and R. J. Hyndman, "Short-term load forecasting based on a semi-parametric additive model," *IEEE Trans. Power Syst.*, vol. 27, no. 1, pp. 134–141, Feb. 2012.

[16] F. Shu and C. Luonan, "Short-term load forecasting based on an adaptive hybrid method," *IEEE Trans. Power Syst.*, vol. 21, no. 1, pp. 392-401, Feb. 2006.

[17] Y. Goude, R. Nedellec, and N. Kong, "Local short and middle term electricity load forecasting with semi-parametric additive models," *IEEE Trans. Smart Grid*, vol. 5, no. 1, pp. 440–446, Jan. 2014.

[18] A. Michiorri, P. C. Taylor, S. C. E. Jupe, and C. J. Berry, "Investigation into the influence of environmental conditions on power system ratings," in *Proc. Inst. Mech. Eng. Part A J. Power Energy*, Nov. 2009, vol. 223, pp. 743–757.

[19] J. Yi *et al.*, "Distribution network voltage control using energy storage and demand side response," in *Proc. 3rd IEEE PES Int. Conf. Exhib. Innovative Smart Grid Technol. (ISGT Europe'12)*, 2012, pp. 1–8.
[20] P. F. Lyons *et al.*, "Design and analysis of electrical energy storage demonstration projects on UK distribution networks," *Appl. Energy*, vol. 137, pp. 677–691, Jan. 2015.
[21] B. F. Wollenberg and A. J. Wood, *Power Generation, Operation, and Control*. Hoboken, NJ, USA: Wiley, 1996.
[22] R. Baldick, "Variation of distribution factors with loading," *IEEE Trans. Power Syst.*, vol. 18, no. 4, pp. 1316–1323, Nov. 2003.
[23] D. Bertsimas and M. Sim, "The price of robustness," *Oper. Res.*, vol. 52, pp. 35–53, Jan./Feb. 2004.
[24] Northern Powergrid. (Apr. 2015). *Customer Led Network Revolution* [Online]. Available: http://www.networkrevolution.co.uk/
[25] D. M. Greenwood *et al.*, "A comparison of real-time thermal rating systems in the U.S. and the U.K.," *IEEE Trans. Power Del.*, vol. 29, no. 4, pp. 1849–1858, Aug. 2014.
[26] Energy Networks Association (ENA), "Engineering recommendation P27: Current rating guide for high voltage overhead lines operating in the UK distribution system," 1986.
[27] P. Mathiesen, J. M. Brown, and J. Kleissl, "Geostrophic wind dependent probabilistic irradiance forecasts for coastal california," *IEEE Trans. Sustain. Energy*, vol. 4, no. 2, pp. 510–518, Apr. 2013.
[28] D. Saez, F. Avila, D. Olivares, C. Canizares, and L. Marin, "Fuzzy prediction interval models for forecasting renewable resources and loads in microgrids," *IEEE Trans. Smart Grid*, vol. 6, no. 2, pp. 548–556, Mar. 2015.

Jialiang Yi (S'12) received the M.Sc. degree in sustainable energy technology from Southampton University, Southampton, U.K. He is currently pursuing the Ph.D. degree in the field of power systems engineering with Newcastle University, Newcastle Upon Tyne, U.K. His research interests include electrical energy storage systems and demand side response in distribution networks.

Pádraig F. Lyons (M'10) received the B.E. degree in electrical and electronic engineering and the M.Eng.Sc. degree in electrical engineering (range extender hybrid electric vehicles) from the University College Cork, Cork, Ireland, and the Ph.D. degree from Durham University, Durham, U.K., in 1999, 2002, and 2010, respectively. His research interests include the area of centralized and distributed control of distributed energy resources, using hardware (laboratory) and software simulation, in future LV networks. He is a Chartered Engineer and a Lecturer with Newcastle University, Newcastle Upon Tyne, U.K.

Peter J. Davison received the B.Eng. and M.Sc. degrees from Durham University, Durham, U.K., in 2010 and 2011, respectively. He is currently pursuing the Ph.D. degree in smart grids. His research interests include real time thermal ratings and domestic load modeling.

Pengfei Wang (S'11) received the M.Sc. degree in electrical power engineering from TU Darmstadt University, Darmstadt, Germany, in 2010. He is currently pursuing the Ph.D. degree in power systems engineering at Newcastle University, Newcastle Upon Tyne, U.K. His research interests include microgeneration systems and voltage control in distribution networks.

Philip C. Taylor (SM'12) received the Engineering Doctorate degree in intelligent demand side management techniques from the University of Manchester Institute of Science and Technology (UMIST), Manchester, U.K., in 2001. He joined Newcastle University, Newcastle-Upon-Tyne, U.K., in April 2013, where he was appointed as the Director of the Institute for Sustainability, a Professor of Electrical Power Systems, and also tasked with overseeing the Science Central development. He previously held the DONG Energy Chair in Renewable Energy, and was the Deputy Director of the Durham Energy Institute and the Director of the Multidisciplinary Centre for Doctoral Training in Energy.